Biochimica et Biophysica Acta 1857 (2016) 387–395

Contents lists available at ScienceDirect

Biochimica et Biophysica Acta

journal homepage: www.elsevier.com/locate/bbabio

Structural and functional characterization of phosphomimetic mutants of cytochrome *c* at threonine 28 and serine 47

Alejandra Guerra-Castellano [a], Irene Díaz-Moreno [a,*], Adrián Velázquez-Campoy [b,c,d], Miguel A. De la Rosa [a], Antonio Díaz-Quintana [a]

[a] Instituto de Bioquímica Vegetal y Fotosíntesis (IBVF), Centro de Investigaciones Científicas Isla de la Cartuja (cicCartuja), Universidad de Sevilla, Consejo Superior de Investigaciones Científicas (CSIC), Avda. Américo Vespucio 49, Sevilla 41092, Spain
[b] Institute of Biocomputation and Physics of Complex Systems (BIFI)-Joint Unit BIFI-IQFR (CSIC), Universidad de Zaragoza, Mariano Esquillor s/n, 50018 Zaragoza, Spain
[c] Departamento de Bioquímica y Biología Molecular y Celular, Universidad de Zaragoza, Pedro Cerbuna 12, 50009 Zaragoza, Spain
[d] Fundacion ARAID, Government of Aragon, Maria de Luna 11, 50018 Zaragoza, Spain

ARTICLE INFO

Article history:
Received 17 October 2015
Received in revised form 15 January 2016
Accepted 20 January 2016
Available online 22 January 2016

Keywords:
Caspase activity
Cytochrome *c*
Electron transport chain
Liposomes binding
Peroxidase activity
Phosphorylation

ABSTRACT

Protein function is frequently modulated by post-translational modifications of specific residues. Cytochrome *c*, in particular, is phosphorylated *in vivo* at threonine 28 and serine 47. However, the effect of such modifications on the physiological functions of cytochrome *c* – namely, the transfer of electrons in the respiratory electron transport chain and the triggering of programmed cell death – is still unknown. Here we replace each of these two residues by aspartate, in order to mimic phosphorylation, and report the structural and functional changes in the resulting cytochrome *c* variants. We find that the T28D mutant causes a 30-mV decrease on the midpoint redox potential and lowers the affinity for the distal site of *Arabidopsis thaliana* cytochrome c_1 in complex III. Both the T28D and S47D variants display a higher efficiency as electron donors for the cytochrome *c* oxidase activity of complex IV. In both protein mutants, the peroxidase activity is significantly higher, which is related to the ability of cytochrome *c* to leave the mitochondria and reach the cytoplasm. We also find that both mutations at serine 47 (S47D and S47A) impair the ability of cytoplasmic cytochrome *c* to activate the caspases cascade, which is essential for triggering programmed cell death.

1. Introduction

Post-translational modifications of proteins are relevant regulatory mechanisms to control an ample set of cell metabolic processes. One of the most usual modifications is phosphorylation. Besides the concomitant change in electrostatics, phosphorylation may alter the structural features of proteins [1] and affect the interactions with their partners [2]. Phosphorylation is modulated by kinases and phosphatases, which are regulated by redox signaling [3–5]. The latter is important in the context of mitochondria, which constitute the main source of reactive oxygen/nitrogen species (RNOS) in the cell [6].

Cytochrome *c* (Cyt *c*) is a small soluble heme-protein localized in the mitochondrial intermembrane space under homeostatic conditions [7]. It takes part in the electron transport chain (ETC), carrying electrons from the cytochrome bc_1 complex (Cyt bc_1) to cytochrome *c* oxidase (COX). Recently, nuclear magnetic resonance (NMR) and computational data revealed that cytochrome c_1 (Cyt c_1), a subunit of Cbc_1, has two binding sites for Cyt *c*. The first site – the so-called proximal site – is located near the heme and is compatible with electron transfer. The second site – the so-called distal site – lays far from the heme and it has been proposed to be a local energy minimum in the restrained Cyt *c* diffusion pathway towards COX [8,9]. Notably, Cyt *c* also interacts with two binding sites on COX [9]. However, the surface regions on Cyt *c* responsible for binding to Cyt c_1 [8,9] and COX [10] are different. Under severe oxidative stress conditions, Cyt *c* exits mitochondria and acts as a programmed cell death (PCD) inductor by interacting with several proteins in the cytoplasm and the nucleus [11–15]. The first reported cytoplasmic interaction of Cyt *c* was with the apoptosis protease activation factor-1 (Apaf-1), which is responsible for the apoptosome assembly and subsequent activation of caspases [16,17]. The apoptosis-inducing form of Cyt *c* has been suggested to be membrane-bound [18–21]. Indeed, a substantial population of Cyt *c* is bound to cardiolipin (CL) in the mitochondrial inner membrane [22].

Abbreviations: Ac-DEVD-AMC, acetyl-Asp-Glu-Val-Asp-7-amino-4-methylcoumarin; Apaf-1, apoptosis protease activation factor-1; Cyt bc_1, cytochrome bc_1 complex; Cyt *c*, cytochrome *c*; Cyt c_1, cytochrome c_1; COX, cytochrome *c* oxidase; CD, circular dichroism; CHAPS, 3-[(3-cholamidopropyl)dimethylammonio]-1-propanesulfonate; CL, cardiolipin; DOPC, 1,2-dioleoyl-sn-glycero-3-phosphocholine; DSC, differential scanning calorimetry; E'_0, midpoint reduction potential; EMSA, electrophoretic mobility shift assay; ETC, electron transfer chain; H_2DCF, dichlorofluorescein diacetate; HEK, human embryonic kidney; ITC, isothermal titration calorimetry; MD, molecular dynamics; NMR, nuclear magnetic resonance; RMSD, root mean square deviation; T_m, midpoint melting temperature; PCD, programmed cell death; TOCL, 1,1′2,2′-tetraoleoylcardiolipin.

* Corresponding author.
E-mail address: idiazmoreno@us.es (I. Díaz-Moreno).

http://dx.doi.org/10.1016/j.bbabio.2016.01.011
0005-2728/

Binding to CL results in a conformational change in the protein [23–25] allowing the entry of a hydrogen peroxide molecule [26]. This enhances the peroxidase activity of Cyt *c* [19,27], so favoring CL oxidation and the release of Cyt *c* to the cytosol [28,29]. Both functions are regulated by post-translational modifications, such as nitration [30–32] or phosphorylation [33–35].

Phosphorylation of Cyt *c* accompanies several pathological situations, including ischemia or cancer [36,37]. *In vivo*, Cyt *c* is phosphorylated in Tyr48 and Tyr97 [33,35]. Tyrosine phosphorylations of Cyt *c* have been classically studied by Tyr to Glu mutation [38,39]. However, this change causes a substantial decrease in the residue volume and surface area. To solve this problem, a new approach based in the Evolved tRNA Synthetase Technique has been lately published [40]. Recently, two additional phosphorylation sites at Thr28 and Ser47 have been reported in the human skeletal muscle [41] (Fig. S1A). Nonetheless, how these modifications affect the structure and the function of Cyt *c* remains unclear. The difficulty of the analysis is that the specific Cyt *c*-phosphorylating kinase remains unknown and isolated Cyt *c* does not preserve the *in vivo* phosphorylation at these positions.

In this work, we analyze two phosphomimetic mutants of human Cyt *c* in which Thr28 or Ser47 are replaced by aspartate (T28D and S47D, respectively). For comparative purposes, two other mutants at the same positions (T28A and S47A) were analyzed to differentiate the effects due to the presence of a negatively charged residue. We show that none of these amino acid substitutions affect the overall structure of Cyt *c*. However, the T28D mutation alters the ability of Cyt *c* to bind to the distal site of *Arabidopsis thaliana* Cyt c_1 and diminishes its redox potential, whereas its oxidation *in vitro* by COX becomes more efficient. In addition, mutations on Ser47 affect the functionality of Cyt *c* in terms of peroxidase activity and ability for caspase activation.

2. Materials and methods

2.1. Site-directed mutagenesis, protein expression and purification of recombinant proteins

Genetic manipulations were performed on a pBTR-1 plasmid (pCyt*c*WT) comprising the CYCS and CYC3 genes, coding for human Cyt *c* and the yeast Cyt *c* heme lyase, respectively. The last enzyme is required for the proper cytoplasmic maturation of human Cyt *c*. Endogenous *c*-type cytochromes in *Escherichia coli* are usually exported to the periplasm space. However, the sequences of the above recombinant gene lacked topogenic sequences, thereby avoiding the export of the gene products to periplasm. Then, the resulting proteins were located in the bacterial cytoplasm. The selectable marker of pCytcWT was a cassette that conferred ampicillin resistance to cells containing this plasmid [42]. pCyt*c*WT was mutated by replacing the ACC triplet coding Thr28 and GGC triplet coding Ser47 in CYCS gene – coding Cyt *c* – with GAT to obtain T28D and S47D, and with GCG to T28A and S47A mutants, respectively. For this purpose, the one-step mutagenic PCR with Accusure™ DNA Polymerase (Bioline) was used following manufacturer's instructions. *E. coli* DH5α was used as a host in all cloning procedures. Plasmid DNA was transferred to *E. coli* strain following the standard heat-shock transformation method. In all cloning procedures involving PCR amplification, the sequences of the amplified fragments were checked with the aid of a commercial sequencing service (StabVida, Caparica, Portugal). The new plasmids, containing the mutated sequences, were called, pCyt*c*T28D, pCyt*c*S47D, pCyt*c*T28A and pCyt*c*S47A. The primers for mutagenic PCR were the following ones:

5-AAACACAAAGATGGTCCCAAC-3 (pCyt*c*T28D forward);
5-GTTGGGACCATCTTTGTGTTT-3 (pCyt*c*T28D reverse);
5-AAACACAAAGCGGGTCCCAAC-3 (pCyt*c*T28A forward);
5-GTTGGGACCCGCTTTGTGTTT-3 (pCyt*c*T28A reverse);
5-CCGGGCTACGATTACACGGCG-3 (pCyt*c*S47D forward);
5-CGCCGTGTAATCGTAGCCCGG-3 (pCyt*c*S47D reverse);
5-CCGGGCTACGCGTACACGGCG-3 (pCyt*c*S47A forward);
5-CGCCGTGTACGCGTAGCCCGG-3 (pCyt*c*S47A reverse).

In order to obtain the four human Cyt *c* mutants T28D, S47D, T28A and S47A, *E. coli* BL-21 (DE3) cells were transformed with the plasmids pCyt*c*T28D, pCyt*c*S47D, pCyt*c*T28A and pCyt*c*S47A, respectively. Cells were cultured for 24 h at 30 °C and 150 rpm in LB rich media supplemented with ampicillin and δ-aminolevulinic acid at final concentrations of 0.1 mg mL^{-1} and 0.1 mM, respectively. Cells were collected by centrifugation (9,000*g* for 10 min), and then resuspended in 1.5 mM borate buffer pH 8.5 (10 mL of buffer per 1 L of culture), supplemented with 1 mM PMSF, 0.02 mg mL^{-1} DNase and 0.2 mg mL^{-1} lysozyme. The cytoplasmic fraction was obtained by sonication on a BRANSON Digital Sonifier® cell disrupter. The cells were intermittently sonicated on ice for 30 s with 60 s allowed for cooling and a 40% vibration amplitude. The total sonication time was 4 min. The resulting suspension was centrifuged at 20,000*g* for 15 min. Then, the supernatant was collected and loaded onto a carboxymethyl cellulose ion exchange column (Sigma® C-4146) pre-equilibrated with 1.5 mM borate buffer pH 8.5. The different mutants of Cyt *c* were eluted from the column along a 36–360 mM NaCl gradient and tested by UV–Vis spectrophotometry in a Jasco V-650 apparatus. The A_{280}/A_{550} ratio of the resulting Cyt *c* preparations in the reduced state was *ca.* 1.0, as previously described [30]. Tryptic digestion and MALDI-TOF analysis (Brüker Daltonics, Germany) confirmed the molecular mass and the different substitutions for each mutant. Protein concentrations were determined by visible spectrophotometry, using an extinction coefficient of 29 mM^{-1} cm^{-1} at 550 nm wavelength for the reduced Cyt *c* species.

2.2. Circular dichroism spectroscopy

All circular dichroism (CD) spectra were recorded using a Jasco J-815 spectropolarimeter equipped with a Peltier temperature-control system. CD intensities are presented in terms of molar ellipticity [θ_{molar}] using molar protein concentration [43]. The secondary structure analyses were carried out by recording far-UV CD spectra (185–250 nm) at 25 °C in a 1-mm quartz cuvette. Samples contained 3 μM protein in 10 mM sodium phosphate pH 6.5, supplemented with 10 μM potassium ferricyanide. For each sample, 20 scans were averaged and analyzed using the CDpro software package [44,45] with the SMP50 and SP37A reference set, as well as with the CLSTR option to compare with a set of proteins with similar folds.

The coordination of the heme iron atom to the S_δ atom of Met80 – the sixth axial ligand of heme group – was analyzed by visible (B-band) recording visible CD spectra (300–600 nm) at 25 °C in a 10-mm quartz cuvette, as previously reported [46]. Samples contained 30 μM protein in 10 mM sodium phosphate pH 6.5, supplemented with 100 μM potassium ferricyanide.

Thermal unfolding was monitored between 20 and 105 °C (with a heating rate of 1 °C/min) by recording the CD signal at far-UV in a 10-mm quartz cuvette. For these assays, the oxidized Cyt *c* species were at 3 μM final concentration in 10 mM sodium phosphate pH 6.5 supplemented with 10 μM potassium ferricyanide. Changes in the tertiary structure of the protein upon increasing the temperature were simultaneously monitored by measuring the changes in total fluorescence at 270 nm excitation wavelength, which are attributed to the exposure of Trp59 to the solvent [47]. The sample mixture contained 30 μM Cyt *c* in 10 mM sodium phosphate pH 6.5 and 100 μM potassium ferricyanide. The experimental data were fitted to a two state native-denatured equilibrium model.

2.3. Electronic absorption spectroscopy

The coordination of the heme group of Cyt *c* was analyzed by monitoring the absorption changes at 699 nm, indicative of the heme Fe–Met80(Sδ) bond [48]. Electronic absorption spectra were recorded in the 600–750 nm range, using a Jasco V-650 spectrophotometer in a 1 mL quartz cuvette with a path length of 10-mm, as previously published [30]. Samples contained 0.2 mM oxidized Cyt *c* in 10 mM sodium phosphate pH 6.5, supplemented with 0.2 mM potassium ferricyanide. For pH titration studies, the pH of each sample was adjusted to the reported values by adding aliquots of 0.1–0.5 M NaOH or 0.1–0.5 M HCl. The full data set was fitted to the Henderson–Hasselbalch function to obtain the pK_a values.

2.4. Potentiometric measurements

The midpoint reduction potentials (E'_0) of the Cyt *c* species were determined as described previously [49]. We measured the differential absorbance at 550–556 nm in a diode-array spectrophotometer (Hewlett Packard 8452 A) and monitoring the redox potential with a Pt–Ag/AgCl combined electrode (Microelectrodes, Inc.) under argon atmosphere. The reaction mix (a volume of 2.5 mL) contained 10 μM Cyt *c* in 50 mM sodium phosphate pH 7, supplemented with 50 μM sodium ascorbate to fully reduce the protein. Quinhydrone ($E'_{m,7} = +280$ mV) was used as a reference compound.

2.5. Calorimetry measurements

Isothermal titration calorimetry (ITC) experiments were performed using an Auto-ITC200 microcalorimeter (MicroCal, GE Healthcare) at 25 °C by titrating *Arabidopsis thaliana* Cyt c_1 on human Cyt *c* species. To avoid additional heat coming from the electron transfer process and redox mediator equilibria, the two samples were reduced and dialyzed against the same buffer before the experiment. The reference cell was filled with distilled water. The experiments consisted of 2 μL injections of 0.4 mM Cyt *c* solution in 10 mM potassium phosphate buffer pH 7.4 into the sample cell initially containing 20 μM Cyt c_1 solution in the same buffer. All solutions were degassed before the titrations were performed. Titrant was injected at appropriate time intervals (150 s) to ensure the thermal power signal returned to the base line prior to the next injection. To achieve homogeneous mixing in the cell, the stirring speed was kept constant at 1,000 rpm. The data, specifically the heat per injection normalized per mol of injectant *versus* molar ratio, were analyzed with Origin 7 (OriginLab) using a two-site binding model with distinct affinity for each site, as recently reported for the *Arabidopsis thaliana* Cyt c_1-Cyt *c* complex [8]. Calibration and performance tests of the calorimeter were carried out conducting $CaCl_2$-EDTA titrations with solutions provided by the manufacturer.

Differential scanning calorimetry (DSC) analyses were performed in a nano DSC (TA instruments) calorimeter. To ensure equilibrium reversibility, 25 μM Cyt *c* samples were prepared in 50 mM glycine buffer, pH 3.5. A temperature interval from 25 to 100 °C was swept at 1 °C min^{-1} rate in every experiment. Data were analyzed by using Nanoanalyze software (TA instruments).

2.6. Liposome preparation and binding experiments

In order to analyze the interaction of Cyt *c* with cardiolipin (CL), small unilamellar liposomes were formed by sonication in 25 mM HEPES buffer pH 7.4. Liposomes were prepared from 1,2-dioleoyl-sn-glycero-3-phosphocholine (DOPC) and 1,1′2,2′-tetraoleoylcardiolipin (TOCL) (4:1 ratio) or DOPC alone (manufactured by Avanti Polar Lipids®).

Cyt *c*:CL binding assays were performed as previously described [27] with minor modifications. Cyt *c* and liposomes were incubated at different ratios for 1 h in 25 mM HEPES buffer pH 7.4. The samples were applied onto 0.8% agarose gel and the electrophoresis was run for 90 min at 50 V in non-denaturing 35 mM HEPES buffer pH 7.4. Gels were stained for protein with 0.25% Coomassie Brilliant Blue R-250 in 45% methanol and 10% acetic acid.

2.7. Peroxidase assays

Peroxidase assays of Cyt *c* were performed as previously described [27]. DOPC:TOCL liposomes were incubated for 1 h at room temperature with Cyt *c* in a ratio 1:100 (*w*/*w*) (Cyt *c*:liposomes) in 20 mM HEPES buffer pH 7.4. After the incubation, and immediately before starting the measurement, 5 μM of 2′,7′-Dichlorofluorescein diacetate (H_2DCF) and 100 μM hydrogen peroxide were added to the samples. DCF fluorescence increment was measured for 30 min using an excitation wavelength of 502 nm and emission of 522 nm (with a slit of 5 nm in both cases) in a Cary Eclipse (Varian) fluorescence spectrophotometer, estimating the peroxidase activity as the slope of fluorescence increment. To test the basal peroxidase activity of Cyt *c*, control assays without liposomes were also performed.

2.8. Caspase activation assays

In vitro activation of caspases was achieved as formerly described [50] with slight changes. Cytoplasmic cell fractions devoid of intrinsic Cyt *c* of human embryonic kidney 293 (HEK 293) were obtained as previously described [38] with minor modifications. After trypsinization, cells were collected by centrifugation (2,000*g* for 5 min). Pellets were washed twice with PBS and one wash with cell extract buffer (CEB: 20 mM HEPES, pH 7.5, 10 mM KCl, 1.5 mM $MgCl_2$, 1 mM EDTA, 1 mM EGTA, 1 mM dithiothreitol, 100 μM PMSF). After these washes, cells were again collected by centrifugation (2,000*g* for 5 min) and pellets were resuspended with two volumes of CEB and were transferred to a Dounce homogenizer. The cell solution was incubated for 15 min at 4 °C. Subsequently, cells were disrupted by 30 strokes with a tight pestle. Lysates were centrifuged at 15,000*g* for 15 min at 4 °C to remove nuclei and organelles. Protein concentration of the extracts was measured using the Bradford protein assay (Bio-Rad, Hercules, CA). 100 μg of cytoplasmic cell fractions was incubated with 1 μM of reduced Cyt *c* species for 60 min at 37 °C in a total volume of 25 μL with 25 mM KCl, 0.2 mM DTT and 0.2 mM dATP. After the incubation, 180 μL of buffer A [10 mM HEPES, pH 7.0, with 50 mM NaCl, 40 mM β-glycerophosphate, 2 mM $MgCl_2$, 5 mM EGTA, 0.1 mg mL^{-1} bovine serum albumin, and 0.1% (*w*/*v*) 3-[3-cholamidopropyl) dimethylammonio]-1-propanesulfonate (CHAPS)], supplemented with 10 μM of acetyl-Asp-Glu-Val-Asp-7-amino-4-methylcoumarin (Ac-DEVD-AMC), a fluorescent substrate specific for caspases 3/7, was added to the reaction mixture and measured immediately. The increase in fluorescence resulting from Ac-DEVD-AMC cleavage was determined in a Cary Eclipse (Varian) fluorescence spectrophotometer (optical slits of 5 nm), using an excitation wavelength of 360 nm and an emission wavelength of 460 nm. Experimental data were derived from the averages of at least three independent experiments.

2.9. Cytochrome c oxidase measurements

To assess the functionality of phosphomimicking Cyt *c* species, we tested their ability to reduce bovine COX *in vitro* using a COX activity kit (Sigma®). The activity was measured spectrophotometrically in a Jasco V-650 spectrophotometer according to the manufacturer's instructions. The initial slopes of at least three independent kinetic traces monitored at 550 nm were measured, and their average was taken as a value for COX activity in terms of Cyt *c* oxidation rate.

2.10. Molecular dynamics simulations

Molecular dynamics (MD) computations were performed using the AMBER12 package [51] and the AMBER 96 force field [52]. All calculations were run under periodic boundary conditions using an orthorhombic (minimum distance between protein and cell faces was initially set to 10 Å) cell geometry and particle mesh Ewald (PME) electrostatics with an Ewald summation cutoff of 9 Å. Autenrieth's force field parameters were used for the oxidized heme moiety [53]. The crystallographic coordinates of human Cyt *c*, including water molecules [pdb code 3zcf] [54] were the starting structure for simulations of the WT species, and the template to model the single-amino acid modifications. Chloride counter-ions were added to neutralize charges. Energy minimization, temperature equilibration, production runs and trajectory analyses were performed as described previously [39,55].

3. Results and discussion

3.1. Physicochemical properties of WT and mutant cytochrome c species

To understand how phosphorylation at positions 28 and 47 affects the properties of Cyt *c*, we have resorted to substitute the corresponding amino acid by aspartate, which mimics the charge change induced by post-translational modification. All mutants showed the typical visible spectra of *c*-type cytochromes (Fig. S1B). To confirm the different mutations, the modified Cyt *c* species were purified to homogeneity (Fig. S1C) and their molecular mass was compared to that of WT Cyt *c* by MALDI-TOF (Fig. S1D). To check whether the amino acid substitutions affected the secondary structure, we recorded CD spectra of every mutant in the far-UV region. All the mutants conserved the overall secondary structure of Cyt *c*, as inferred from the far-UV CD spectra, although the random fraction increased in the case of S47A mutant (Fig. 1 top, Fig S2).

In the native form, the heme iron of Cyt *c* is hexacoordinated, His18 and Met80 providing the fifth and sixth ligands, respectively [56]. Subtle changes in the heme crevice are able to affect the heme properties. Hence, we recorded visible CD spectra in the Soret region to detect changes in the heme iron coordination [57]. All species, except S47A mutant, showed the distinctive CD spectrum for Cyt *c* state III, with a maximum at 410 nm corresponding to the B-band [58] (Fig. 1 bottom). The splitting observed in this B-band is due to internal electric field of the protein, and it is usually observed in low-spin cytochromes [59]. Interestingly, T28D mutant showed a lower amplitude of the B-band, which is attributed to a Stark effect that depends on the orientation of the internal electric field with respect to the axes defined by the equatorial ligands. T28D mutation locates at the rim of the heme cleft, introducing a negative charge in the vicinity of the delta-*meso* position [60]. Such B-band splitting was fully lost in the S47A mutant. To assess this behavior of the mutation by alanine at position 47 and to compare it to the WT protein, molecular dynamics (MD) computations were performed on the native WT and S47A species. In agreement with UV-CD data, the structure is maintained along both, WT and S47A computations. The average of the root mean square deviation (RMSD) values for the protein main chain atoms with respect to the energy minimized structure were 0.83 Å and 0.79 Å, respectively. The backbone RMSD between the two average structures was 0.27 Å. Still, surface sidechains changed slightly: Both proteins showed 17 salt bridges, but 3 of them were different. Glu104-Lys100, Glu90-Lys13 and Glu4-Lys100 were observed in the WT form but not in the mutant. Conversely, Glu66-Arg91, Glu69-Lys88 and Glu4-Lys5 appeared in the S47A mutant, but were not detected in the WT species.

As regards atomic fluctuations, the overall statistics were almost identical for the two proteins even when computed for all atoms (Fig 2). In fact, their average values were equal, according to *t*-Student tests at 0.95 significance. However, several atoms changed their dynamic behavior. Among them, the sidechains of Lys53, Asn54, heme

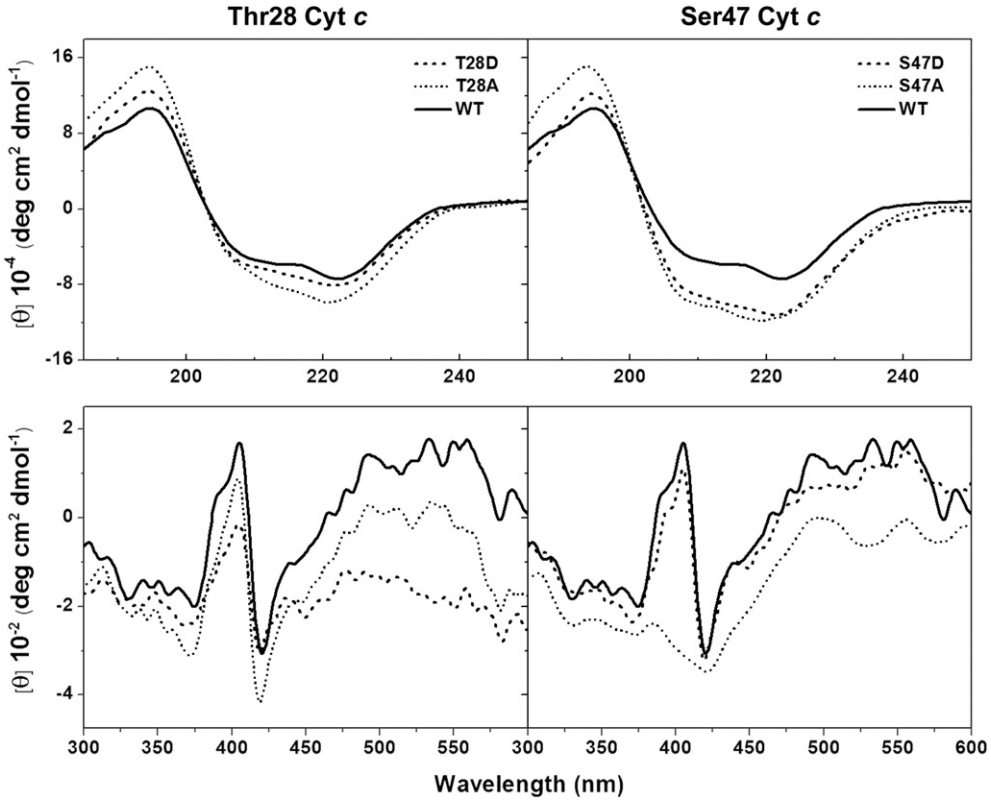

Fig. 1. Far-UV (top) and visible CD spectra (bottom) of WT and phosphomutant species of Cyt *c*. The T28D, T28A, S47D and S47A variants were analyzed in comparison with WT Cyt *c*. All measurements were recorded on oxidized protein samples.

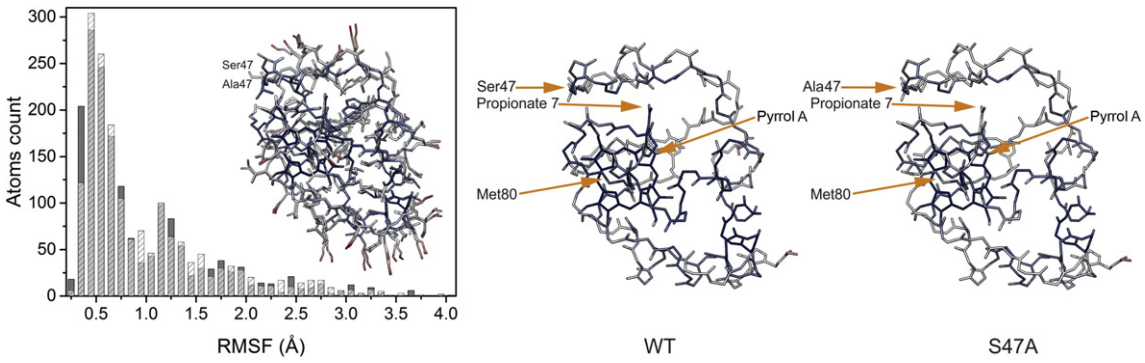

Fig. 2. Atomic fluctuations of WT and S47A Cyt *c* species along MD trajectories. Left. Overlay of the frequency distributions of the atomic root mean square fluctuations (RMSF) obtained from the analysis of the WT and S47A Cyt *c*. Bars corresponding to WT Cyt *c* are in gray. To allow comparison of frequency distributions between WT and mutant species, bars corresponding to the S47A Cyt *c* are in translucent pattern and overlaid onto the WT ones. Inserted in this panel an overlay of the average structures of WT and S47A species, displays all their heavy atoms. Color scales from first (blue) to 99 (red) percentiles of the frequency distribution. White color corresponds to the median value. Right. Detail of the backbone and heme moiety of the two proteins, colored as in the inset of left panel.

propionate 7 and pyrrole A of the cofactor exhibited larger fluctuations in the mutant. In addition, the atomic fluctuations of Arg38 sidechain did not change substantially, but the rotation of its guanidinium group – located 6 Å from heme propionate 7 carboxyl – was impaired (Fig. S3). Actually, its order parameter increased from 0.14 in the WT to 0.39 in the mutant, and the correlation time rose from 117 ps to 281 ps. The disturbance of the hydrogen bond between heme propionate 7 and ε-amide of Arg38 have been previously described in G41S mutant of Cyt *c* [59].

To find a correlation between the amino acid substitution and the loss of the CD B-band splitting, we carried out a principal component analysis of the trajectory (Fig. S4). The S47A mutation clearly affected the coupling between the flexible regions motions, namely the nested Ω loop (residues 40–57), the foldon II Ω loop (from Thr19 to Phe36) and the Ω loop of foldon IV (containing Met ligand). The second principal component revealed a coupling between the motions of heme propionate 7, porphyrin ring A, and the nested Ω loop that contains the mutated residue, a finding that is not observed in the WT form. Altogether, these data suggest that the loss of the B-band splitting is due to a change in the motion modes rather than to a substantial structural change.

The oxidized form of Cyt *c* can show distinct conformations along the pH range from 1 to 12, which result from changes in heme axial coordination and/or in protein folding [61]. The transformation of the physiological state III into state IV upon a pH increase is called alkaline transition [62] and involves a replacement of Met80 as axial ligand by Lys72, Lys73 or Lys79 [63,64]. As this transition has been related to a change in the Cyt *c* cell location [65], we tested whether any of the mutations affected the pK_a of this transition by inspecting the charge transfer band at 699 nm [66]. The pK_a values of WT Cyt *c* is *ca.* 9.5 [30]. The phosphomimicking Cyt *c* species in Tyr48 decreases the pK_a to a physiological value [39,40]. Opposite, the pK_a for the alkaline transition proved to be insensitive to the mutations of residues 28 and 47 (Table 1, Fig. S5). This is in agreement with the orientation of the side chains of alanine and aspartate at these positions, which point both outside the protein (Fig. S1A) and do not affect the H-bond network around the heme moiety. Alkaline transition was reversible for all Cyt *c* samples.

3.2. Thermal stability of cytochrome c mutants

The axial ligands and the surrounding residues of the heme group play crucial roles in conformational stability of Cyt *c* [67]. This relies on the H-bonding network, steric restrictions and hydrophobic interactions, among other factors. Changes in the sequence of the protein can also induce changes in its midpoint melting temperature (T_m). The thermal stability was studied by far-UV CD and fluorescence, respectively.

Previous work of our group has described temperature-dependent changes in the coordination of the heme group in other phosphomimicking Cyt *c* mutants at position Tyr48 and Tyr97 that affect the T_m value [39,40]. In this case, all mutants show similar T_m values to WT Cyt *c* (Table 2). Still, fluorescence data reveal that S47A shows an unfolding transition with a T_m value of *ca.* 20 °C lower than that of the WT species (Table 2). This indicates that the mutation affects the stability of the region surrounding Trp59, which is close to Arg38 and heme propionate 7. To dig into this subject, the thermal stability of WT and S47A was also tested by DSC. In both cases the T_m value was similar; however, the unfolding of the WT species was reversible but that of the mutant was not (Fig. S6).

3.3. Interaction of cytochrome c mutants with their partners of the electron transport chain

To study the ability of Cyt *c* mutants to act as electron carriers, we analyzed the cross-interaction between *Arabidopsis thaliana* Cyt c_1 and human Cyt *c* by ITC. The overall sequence identity between the soluble domain of human Cyt c_1 and that of the *Arabidopsis* homolog is 62% and, both Cyt c_1, show very similar charge distributions especially at the so-called distal site of Cyt c_1 (Fig. S7). In addition, early analyses by NMR and ITC indicate that *Arabidopsis* Cyt c_1 shows almost identical affinities for the human and *Arabidopsis* Cyt *c* species [8,9]. As described previously for the *Arabidopsis thaliana* Cyt c_1-WT human Cyt *c* complex

Table 1
Biophysical properties of Cyt *c* phosphomutants.

	Alkaline transition pK_a values*	Midpoint redox potential values (E'_0, mV)
WT	9.5 ± 0.2[29]	266.5 ± 2.0[48]
T28D	9.9 ± 0.2	233.1 ± 0.7
T28A	8.9 ± 0.1	253.5 ± 0.8
S47D	9.2 ± 0.1	255.5 ± 1.2
S47A	9.1 ± 0.0	255.5 ± 0.6

* Values determined by optical spectroscopy (A_{699nm}).

Table 2
Midpoint melting temperature (T_m, °C) of Cyt *c* phosphomutants.

	Far UV CD (220 nm)	Fluorescence (270 nm)
WT	86.64 ± 2.13	86.82 ± 0.26
T28D	87.84 ± 2.59	86.62 ± 0.27
T28A	88.65 ± 0.60	85.92 ± 0.35
S47D	87.15 ± 0.71	85.59 ± 0.29
S47A	87.00 ± 2.75	67.02 ± 0.10

[9], the isotherms fit a model with two independent binding sites, for all the phosphomimicking Cyt *c* mutants over Cyt c_1. In Fig. 3A, it is shown that all the interactions were endothermic processes with a low dissociation constant value for the proximal site and a higher value for the distal site of Cyt c_1 (Table S1). Remarkably, the dissociation constant for the T28D mutant over the distal site was eight times larger than for the WT species, whereas the value in the T28A mutant perfectly matches that of the WT (Fig. 3A and Table S1). The effect on the interaction with the distal site of Cyt c_1, driven by electrostatic forces, could be explained because of the presence of a negative charge at this position altering the electrostatic potential (Fig. 3B). In the case of S47A and S47D species, both mutations cause a two-fold increase in K_D values for the distal site (Fig. S8A). Residue 47 is implicated in the interaction surface of Cyt c_1-Cyt *c* complex [9]. Changes in the electrostatic potential, in the case of S47D mutant (Fig. S8B), or in solvation properties of S47A species (Fig. S8C) explained the decrease in the affinity for distal site of Cyt c_1.

Native Cyt *c* has two redox forms, a ferric (Fe^{+3}) oxidized state and a ferrous reduced one (Fe^{+2}). The midpoint redox potential (E'_0) of this pair in human Cyt *c* is +260 mV at pH 7.0 [50]. Changes in the heme moiety induced by mutations may affect the redox potential value of Cyt *c*, thereby altering its efficiency as an electron carrier. We observed that the mutant T28D shows a significant decrease in its E'_0 value in comparison to WT Cyt *c* (*ca.* 30 mV) (Table 1). The drop in E'_0, together with the increase in the distal site K_D value – which supports the "floating boat bridge" model of Cyt *c* [8,9] – could explain a lower efficiency as electron carrier of T28D mutant.

We analyzed the interaction with COX, the other partner of Cyt *c* in the electron transfer chain, by spectrophotometric assay. This allowed observing an increment of *ca.* 70% when a negative charge is present in any of the two positions (Fig. 4). These effects on the COX activity of mutant species suggest that these residues are implicated in the interaction with COX. Notably, Sakamoto and co-workers observed a specific line broadening of Thr28 resonance for the oxidized Cyt *c*-COX complex [10]. However, the authors ruled out these residues being involved in the interaction between Cyt *c* and COX.

Thus, our results suggest that the presence of a negative charge at position 28 of Cyt *c* affects its capacity to transfer electrons between Cyt c_1 and COX. In the case of the mutants at position 47 (S47A and S47D), a negative charge in this position (S47D) increases the electron transfer to the COX.

3.4. Peroxidase activity of cytochrome c mutants and their interaction with cardiolipin

We have analyzed the peroxidase activity of phosphomimicking Cyt *c* species, a property shared by almost all heme-proteins [68]. Some authors have attributed this activity to the formation of a compound I-type intermediate when Cyt *c* reacts with hydrogen peroxide. The peroxidase activity was also related with the alkaline transition [69], as it involves

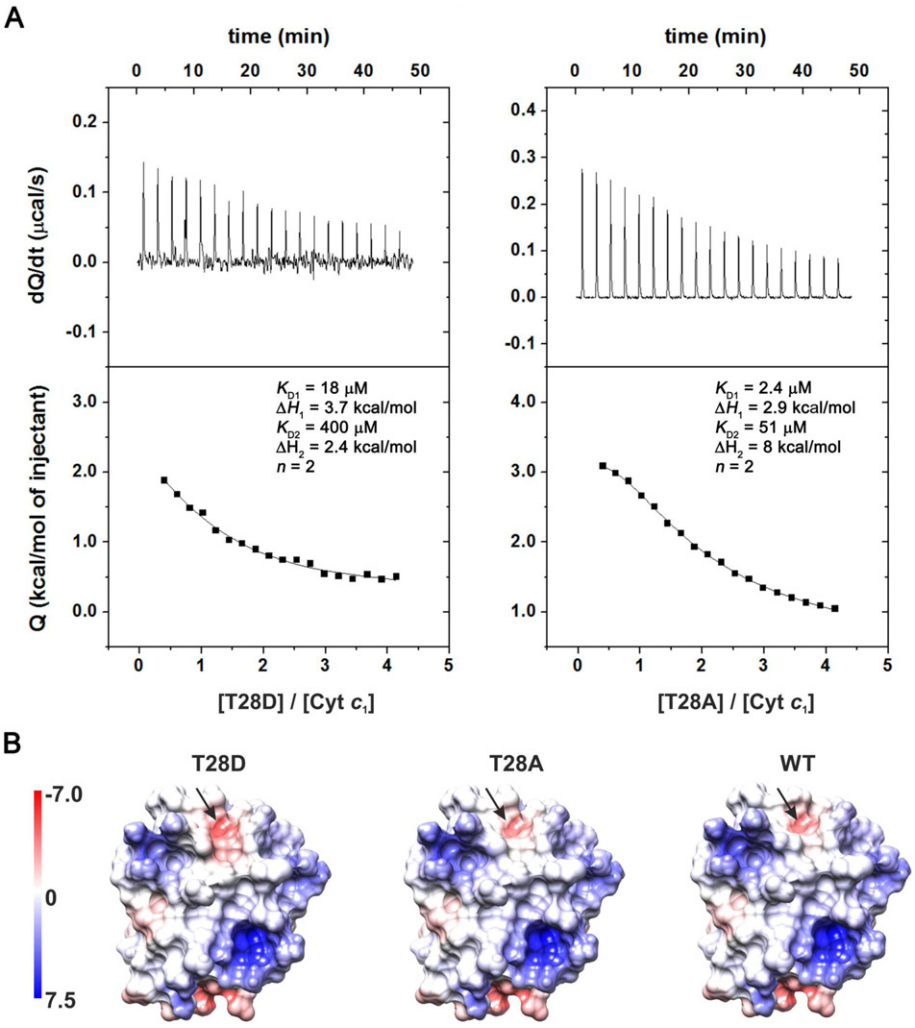

Fig. 3. ITC measurements of reduced T28D-Cyt c_1 and T28A-Cyt c_1 complexes (A) and surface electrostatic potentials of the Cyt *c* species (B). In A, calorimetry experimental data were fitted to a 2:1 binding model. Thermograms are shown at the upper panels and binding isotherms at the lower panels. In B, the simulation was performed using DelPhi aided by Chimera, assuming an ionic strength of 150 mM. The interior and exterior dielectric constants were fixed to 2 and 80, respectively. Arrows show the residue at position 28.

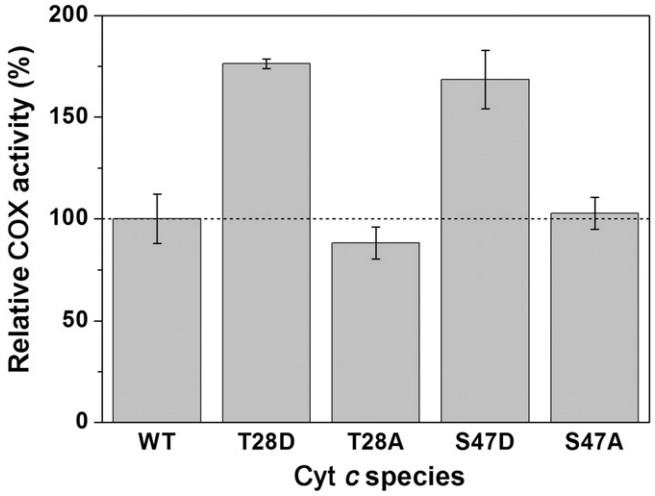

Fig. 4. COX activity of complex IV with WT and mutant Cyt *c* species. The COX activity was measured using a commercial kit (Sigma®). Data represent the mean ± SD of three individual experiments and are normalized to the results with WT Cyt *c*.

the breakage of Fe–Sδ (Met80) bond. However, a poor correlation was found between the populations of high-spin states and the peroxidase activity in a recent analysis that involved tyrosine modifications of Cyt *c* [30]. Recently, it has been demonstrated that Cyt *c* binding to cardiolipin (CL) enhances this activity, due to a conformational change that allows the access of hydrogen peroxide to the heme crevice [70]. In order to analyze the peroxidase activity of Cyt *c* mutants, we studied this activity in the presence of liposomes with and without TOCL, as well as the affinity of the mutant Cyt *c* species towards liposomes. The binding of Cyt *c* to liposomes was examined by electrophoretic mobility shift assay (EMSA) in native agarose gels (Fig. 5A). As expected, free Cyt *c* species moved to the cathode (Fig. 5A, first lane), while Cyt *c*:liposomes complexes migrated to the anode. To compare the binding affinities of the various Cyt *c* species to DOPC or DOPC:TOCL liposomes, we evaluated the free populations of Cyt *c* variants at different protein:lipid ratios from the mobility profiles in the native gel. The EMSA data showed that all Cyt *c* mutants bind to DOPC:TOCL membranes but show small affinities towards DOPC liposomes. The mobility of Cyt *c* decreased at increasing protein-to-lipid ratios, and according to the various affinities towards CL (Fig. 5A). In this regard, the mutations T28D, S47D and S47A – but not T28A – decreased their affinity for CL-containing liposomes, as inferred by the presence of free protein at high lipid concentrations. Strikingly T28A and S47A mutants showed a different behavior in the presence of DOPC liposomes. This may reflect a local change in the surface properties of these proteins.

We measured the peroxidase activity of Cyt *c* either free or bound to DOPC:TOCL liposomes at a 1:100 ratio (Cyt *c*:lipids). In the absence of liposomes, all the phosphomimicking mutants exhibited a peroxidase activity twice that observed for the WT form and the control species (Fig. 5B). The presence of DOCL:TOCL vesicles enhanced the activity of all species, except of S47D mutant, in agreement with the distinct degrees of binding to CL. This explains the small activity increment shown by the T28D mutant, since at 1:100 ratio its free form population is high. The low peroxidase activities of S47D and S47A mutants in the presence of DOPC:TOCL liposomes at Cyt *c*:lipids ratio of 1:100 were also explained by the decrease in the affinity for CL (see gels S47D and S47A in Fig 5A). S47A Cyt *c* (Fig. 5B) showed a larger affinity towards the liposomes than the S47D mutant, especially significant in those liposomes devoid of CL. In this way, a negative charge at position 28 and 47 may produce a structural change that turns the heme group more accessible to hydrogen peroxide, explaining the increment in peroxidase activity in the absence of liposome, compared to WT Cyt *c*. However, this change affected the interaction with CL, maybe blocking the insertion of acyl chain of CL in the hydrophobic pockets of Cyt *c* (Fig. S9) thereby decreasing the affinity for the lipid and affecting the peroxidase activity in its presence. Controls of these experiments were included in Fig. S10.

3.5. Activation of caspases cascade by cytochrome c mutants

During PCD, Cyt *c* is released from mitochondria and interacts with Apaf-1 to form the apoptosome, the caspases-activating platform. We analyzed the capacity of Cyt *c* species to activate caspase 3, considered one of the central molecules in PCD, in cytoplasmic cell extract (see insert in Fig. 6). A negative charge at position 28 did not affect the activity,

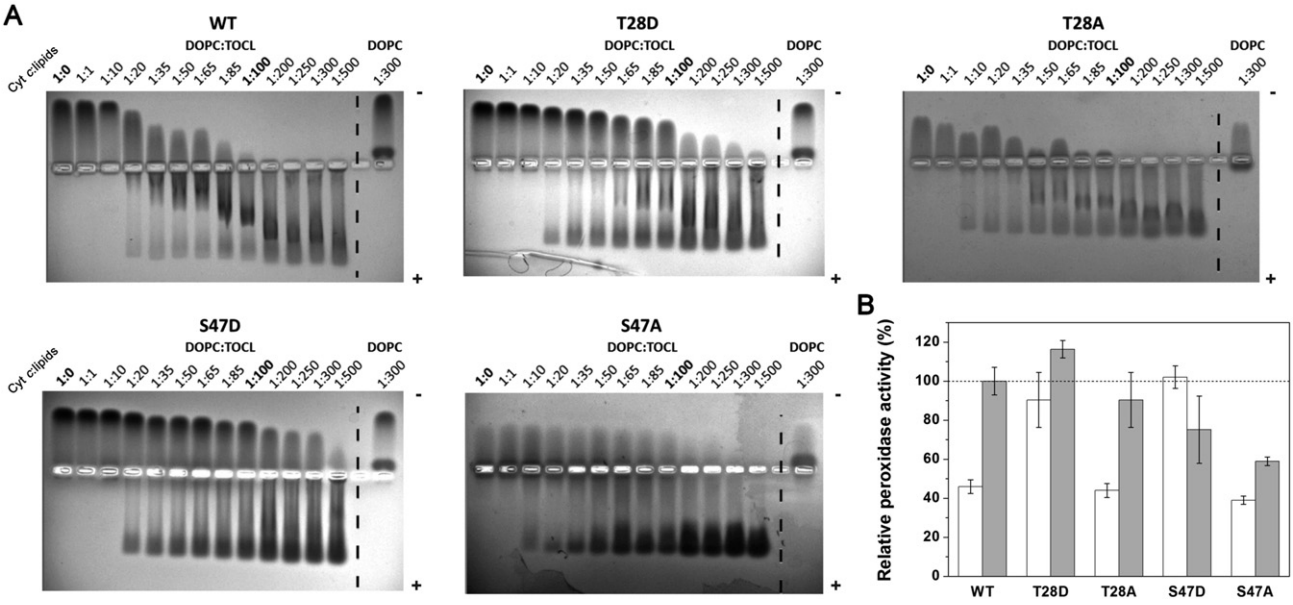

Fig. 5. Liposomes-binding assays and peroxidase activity of WT and mutants Cyt *c* species. A) EMSA of the Cyt *c* species in the presence of increasing concentration of lipids. DOPC:TOCL (4:1) or DOPC liposomes were incubated with WT or phosphomutants of Cyt *c* in 25 mM HEPES buffer, pH 7.4. The samples were loaded onto 0.8% agarose gel. The gels were stained with Coomassie Brilliant Blue. Ratios in bold indicate the Cyt *c*:lipid ratio at which the peroxidase activity was measured. B) Relative peroxidase activities of the Cyt *c* species without liposomes (white column) or in the presence of liposomes containing a mixture of DOPC:TOCL (4:1) (gray column). Data represent the mean ± SD of three individual experiments and are normalized to the results with relative peroxidase activity of WT Cyt *c* in the presence of DOPC:TOCL containing liposomes at a Cyt *c*:lipids ratio of 1:100 (*w*/*w*).

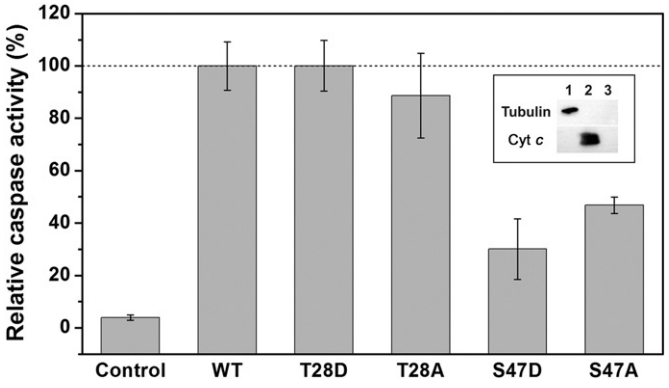

Fig. 6. Caspase activity of WT and mutant Cyt *c* species. Relative caspase activity in HEK293 cytoplasmic cell extracts devoid of intrinsic Cyt *c* was measured upon addition of exogenous Cyt *c*. The Western blots at the inset confirm the lack of endogenous Cyt *c* in the cytoplasmic cell extracts by immunoblotting with anti-tubulin (cytosolic marker) and anti-Cyt *c* antibodies (see insert). Lane 1: cytoplasmic cell extracts; lane 2: Cyt *c*; and lane 3: BSA, as negative control. The caspase auto-activation, without addition of exogenous Cyt *c*, was also tested. Data represent the mean ± SD of three individual experiments and are normalized to the results with WT Cyt *c*.

but both mutants at residue 47 showed a decrease of *ca.* 50% (Fig. 6). Such effect is independent of the additional negative charge concomitant to phosphorylation. Nevertheless, our results suggest that any modification of residue 47 affects the pro-apoptotic function of Cyt *c*. In agreement, a recent report indicates that serine 47 of Cyt *c* is involved in the interaction with several protein related to apoptosis, such as the anti-apoptotic Bcl-xL protein [71]. Similarly, there are other residues of Cyt *c* which play an essential role in apoptotic signaling, such as Gly41 [72–75].

4. Conclusions

Hence, we show that the mutations at residues 28 and 47 keep the overall structure of Cyt *c*. According to the ITC data, the phosphomimicking mutants of Cyt *c* are able to bind to Cyt c_1 with a stoichiometry of 2:1. Whereas the proximal site of Cyt c_1 (compatible with electron transfer) shows a similar affinity for all the species, Cyt *c* docking on the electrostatically-driven distal site of Cyt c_1 is substantially weakened by the presence of a negative charge at position 28 of Cyt *c*. Also, the presence of a negative charge at positions 28 and 47 of Cyt *c* increases the COX activity. In addition, the phosphomimicking Cyt *c* species have altered the affinity to CL and consequently the peroxidase activity of Cyt *c*. Remarkably, the residue 47 has been revealed to be important for caspase activation, and could be a "hot point" of the apoptosis signaling pathway. Still, unveiling the molecular mechanisms by which residue 47 plays this role demands further experiments.

Conflict of interest

All authors declare no conflict of interest.

Transparency document

The Transparency document associated with this article can be found, in online version.

Acknowledgments

This work was supported by the Ministry of Economy and Competitiveness (BFU2012-31670), Ramón Areces Foundation (2015-2017), European Social Fund 2007–2013 (ESF 2007-2013), Andalusian Government (CVI-BIO198), grant JaePre_2011_01248 awarded to A.G.C., Biointeractomics platform (cicCartuja, Seville) and TA Instruments.

Appendix A. Supplementary data

Supplementary data to this article can be found online at http://dx.doi.org/10.1016/j.bbabio.2016.01.011.

References

[1] I. Díaz-Moreno, D. Hollingworth, T.A. Frenkiel, G. Kelly, S. Martin, S. Howell, M. García-Mayoral, R. Gherzi, P. Briata, A. Ramos, Phosphorylation-mediated unfolding of a KH domain regulates KSRP localization via 14-3-3 binding, Nat. Struct. Mol. Biol. 16 (2009) 238–246.
[2] P. Cohen, The regulation of protein function by multisite phosphorylation — a 25 year update, Trends Biochem. Sci. 25 (2000) 596–601.
[3] H.P. Monteiro, A. Stern, Redox modulation of tyrosine phosphorylation-dependent signal transduction pathways, Free Radic. Biol. Med. 21 (1996) 323–333.
[4] L. Liaudet, G. Vassalli, P. Pacher, Role of peroxynitrite in the redox regulation of cell signal transduction pathways, Front. Biosci. 14 (2009) 4809–4814.
[5] A. Corcoran, T.G. Cotter, Redox regulation of protein kinases, FEBS J. 280 (2013) 1944–1965.
[6] J.F. Turrens, Mitochondrial formation of reactive oxygen species, J. Physiol. 552 (2003) 335–344.
[7] P. Delivani, S.J. Martin, Mitochondrial membrane remodeling in apoptosis: an inside story, Cell Death Differ. 13 (2006) 2007–2010.
[8] B. Moreno-Beltrán, A. Díaz-Quintana, K. González-Arzola, A. Velázquez-Campoy, M.A. De la Rosa, I. Díaz-Moreno, Cytochrome c_1 exhibits two binding sites for cytochrome c in plants, Biochim. Biophys. Acta, Bioenerg. 1837 (2014) 1717–1729.
[9] B. Moreno-Beltrán, I. Díaz-Moreno, K. González-Arzola, A. Guerra-Castellano, A. Velázquez-Campoy, M.A. De la Rosa, A. Díaz-Quintana, Respiratory complexes III and IV can each bind two molecules of cytochrome c at low ionic strength, FEBS Lett. 589 (2015) 476–483.
[10] K. Sakamoto, M. Kamiya, M. Imai, K. Shinzawa-Itoh, T. Uchida, K. Kawano, S. Yoshikawa, K. Ishimori, NMR basis for interprotein electron transfer gating between cytochrome c and cytochrome c oxidase, Proc. Natl. Acad. Sci. U. S. A. 108 (2011) 12271–12276.
[11] Y.-L.P. Ow, D.R. Green, Z. Hao, T.W. Mak, Cytochrome c: functions beyond respiration, Nat. Rev. Mol. Cell Biol. 9 (2008) 532–542.
[12] J. Martínez-Fábregas, I. Díaz-Moreno, K. González-Arzola, S. Janocha, J.A. Navarro, M. Hervás, R. Bernhardt, A. Díaz-Quintana, M.A. De la Rosa, New *Arabidopsis thaliana* cytochrome c partners: a look into the elusive role of cytochrome c in programmed cell death in plants, Mol. Cell. Proteomics 12 (2013) 3666–3676.
[13] J. Martínez-Fábregas, I. Díaz-Moreno, K. González-Arzola, S. Janocha, J.A. Navarro, M. Hervás, R. Bernhardt, A. Velázquez-Campoy, A. Díaz-Quintana, M.A. De la Rosa, Structural and functional analysis of novel human cytochrome c targets in apoptosis, Mol. Cell. Proteomics 13 (2014) 1439–1456.
[14] J. Martínez-Fábregas, I. Díaz-Moreno, K. González-Arzola, A. Díaz-Quintana, M.A. De la Rosa, A common signalosome for programmed cell death in humans and plants, Cell Death Dis. 5 (2014), e1314.
[15] K. González-Arzola, I. Díaz-Moreno, A. Cano-González, A. Díaz-Quintana, A. Velázquez-Campoy, B. Moreno-Beltrán, A. López-Rivas, M.A. De la Rosa, Structural basis for inhibition of the histone chaperone activity of SET/TAF-Iβ by cytochrome c, Proc. Natl. Acad. Sci. U. S. A. 112 (2015) 9908–9913.
[16] H. Zou, Y. Li, X. Liu, X. Wang, An APAF-1·cytochrome c multimeric complex is a functional apoptosome that activates procaspase-9, J. Biol. Chem. 274 (1999) 11549–11556.
[17] S. Desagher, J.C. Martinou, Mitochondria as the central control point of apoptosis, Trends Cell Biol. 10 (2000) 369–377.
[18] R. Jemmerson, J. Liu, D. Hausauer, K.P. Lam, A. Mondino, R.D.A. Nelson, Conformational change in cytochrome c of apoptotic and necrotic cells is detected by monoclonal antibody binding and mimicked by association of the native antigen with synthetic phospholipid vesicles, Biochemistry 38 (1999) 3599–3609.
[19] V.E. Kagan, V.A. Tyurin, J. Jiang, Y.Y. Tyurina, V.B. Ritov, A.A. Amoscato, A.N. Osipov, N.A. Belikova, A.A. Kapralov, V. Kini, I.I. Vlasova, Q. Zhao, M. Zou, P. Di, D.A. Svistunenko, I.V. Kurnikov, G.G. Borisenko, Cytochrome c acts as a cardiolipin oxygenase required for release of proapoptotic factors, Nat. Chem. Biol. 1 (2005) 223–232.
[20] A.A. Kapralov, N. Yanamala, Y.Y. Tyurina, L. Castro, A.S. Arias, Y.A. Vladimirov, A. Maeda, A.A. Weitz, J. Peterson, D. Mylnikov, V. Demicheli, V. Tortora, J. Klein-Seetharaman, R. Radi, V.E. Kagan, Topography of tyrosine residues and their involvement in peroxidation of polyunsaturated cardiolipin in cytochrome c/cardiolipin peroxidase complexes, Biochim. Biophys. Acta – Biomembr. 1080 (2011) 2147–2155.
[21] C.L. Bergstrom, P.A. Beales, Y. Lv, T.K. Vanderlick, J.T. Groves, Cytochrome c causes pore formation in cardiolipin-containing membranes, Proc. Natl. Acad. Sci. U. S. A. 110 (2013) 6269–6274.
[22] E.K.J. Tuominen, C.J.A. Wallace, P.K.J. Kinnunen, Phospholipid cytochrome c interaction evidence for the extended lipid anchorage, J. Biol. Chem. 277 (2002) 8822–8826.
[23] P.J.R. Spooner, A. Watts, Reversible unfolding of cytochrome c upon interaction with cardiolipin bilayers. 1. Evidence from deuterium NMR measurements, Biochemistry 30 (1991) 3871–3879.
[24] F. Sinibaldi, B.D. Howes, M.C. Piro, F. Polticelli, C. Bombelli, T. Ferri, M. Coletta, G. Smulevich, R. Santucci, Extended cardiolipin anchorage to cytochrome c: a model for protein-mitochondrial membrane binding, J. Biol. Inorg. Chem. 15 (2010) 689–700.

[25] Y. Hong, J. Muenzner, S.K. Grimm, E.V. Pletneva, Origin of the conformational heterogeneity of cardiolipin-bound cytochrome c, J. Am. Chem. Soc. 134 (2012) 18713–18723.
[26] Y.A. Vladimirov, E.V. Proskurnina, D.Y. Izmailov, A.A. Novikov, A.V. Brusnichkin, A.N. Osipov, V.E. Kagan, Cardiolipin activates cytochrome c peroxidase activity since it facilitates H_2O_2 access to heme, Biochemistry 71 (2006) 998–1005.
[27] N.A. Belikova, Y.A. Vladimirov, A.N. Osipov, A.A. Kapralov, V.A. Tyurin, M.V. Potapovich, L.V. Basova, J. Peterson, I.V. Kurnikov, V.E. Kagan, Peroxidase activity and structural transitions of cytochrome c bound to cardiolipin-containing membranes, Biochemistry 45 (2006) 4998–5009.
[28] S.L. Iverson, S. Orrenius, The cardiolipin–cytochrome c interaction and the mitochondrial regulation of apoptosis, Arch. Biochem. Biophys. 423 (2004) 37–46.
[29] F. Gonzalvez, E. Gottlieb, Cardiolipin: setting the beat of apoptosis, Apoptosis 12 (2007) 877–885.
[30] J.M. García-Heredia, I. Díaz-Moreno, P.M. Nieto, M. Orzáez, S. Kocanis, M. Teixeira, E. Pérez-Payá, A. Díaz-Quintana, M.A. De la Rosa, Nitration of tyrosine 74 prevents human cytochrome c to play a key role in apoptosis signaling by blocking caspase-9 activation, Biochim. Biophys. Acta, Bioenerg. 1797 (2010) 981–993.
[31] I. Díaz-Moreno, J.M. García-Heredia, A. Díaz-Quintana, M. Teixeira, M.A. De la Rosa, Nitration of tyrosines 46 and 48 induces the specific degradation of cytochrome c upon change of the heme iron state to high-spin, Biochim. Biophys. Acta, Bioenerg. 1807 (2011) 1616–1623.
[32] J.M. García-Heredia, I. Díaz-Moreno, A. Díaz-Quintana, M. Orzáez, J.A. Navarro, M. Hervás, M.A. De la Rosa, Specific nitration of tyrosines 46 and 48 makes cytochrome c assemble a non-functional apoptosome, FEBS Lett. 586 (2012) 154–158.
[33] A.R. Lee, K. Salomon, J.W. Yu, L.I. Doan, M. Grossman, Hüttemann, New prospects for an old enzyme: mammalian cytochrome c is tyrosine-phosphorylated in vivo, Biochemistry 45 (2006) 9121–9128.
[34] M. Hüttemann, I. Lee, L. Samavati, H. Yu, J.W. Doan, Regulation of mitochondrial oxidative phosphorylation through cell signaling, Biochim. Biophys. Acta, Bioenerg. 1773 (2007) 1701–1720.
[35] H. Yu, I. Lee, A.R. Salomon, K. Yu, M. Hüttemann, Mammalian liver cytochrome c is tyrosine-48 phosphorylated in vivo, inhibiting mitochondrial respiration, Biochim. Biophys. Acta, Bioenerg. 1777 (2008) 1066–1071.
[36] M. Hüttemann, I. Lee, A. Pecinova, P. Pecina, K. Przyklenk, J.W. Doan, Regulation of oxidative phosphorylation, the mitochondrial membrane potential, and their role in human disease, J. Bioenerg. Biomembr. 40 (2008) 445–456.
[37] M. Hüttemann, I. Lee, L.I. Grossman, J.W. Doan, T.H. Sanderson, Phosphorylation of mammalian cytochrome c and cytochrome c oxidase in the regulation of cell destiny: respiration, apoptosis, and human disease, Adv. Exp. Med. Biol. 748 (2012) 237–264.
[38] P. Pecina, G.G. Borisenko, N.A. Belikova, Y.Y. Tyurina, A. Pecinova, I. Lee, A.K. Samhan-Arias, K. Przyklenk, V.E. Kagan, M. Hüttemann, Phosphomimetic substitution of cytochrome c tyrosine 48 decreases respiration and binding to cardiolipin and abolishes ability to trigger downstream caspase activation, Biochemistry 49 (2010) 6705–6714.
[39] J.M. García-Heredia, A. Díaz-Quintana, M. Salzano, M. Orzáez, E. Pérez-Payá, M. Teixeira, M.A. De la Rosa, I. Díaz-Moreno, Tyrosine phosphorylation turns alkaline transition into a biologically relevant process and makes human cytochrome c behave as an anti-apoptotic switch, J. Biol. Inorg. Chem. 16 (2011) 1155–1168.
[40] A. Guerra-Castellano, A. Díaz-Quintana, B. Moreno-Beltrán, J. López-Prados, P.M. Nieto, W. Meister, J. Staffa, M. Teixeira, P. Hildebrandt, M.A. De la Rosa, I. Díaz-Moreno, Mimicking tyrosine phosphorylation in human cytochrome c by the evolved tRNA synthetase technique, Eur. Chem. J. 21 (2015) 15004–15012.
[41] X. Zhao, I.R. León, S. Bak, M. Mogensen, K. Wrzesinski, K. Højlund, O.N. Jensen, Phosphoproteome analysis of functional mitochondria isolated from resting human muscle reveals extensive phosphorylation of inner membrane protein complexes and enzymes, Mol. Cell. Proteomics 10 (2011) (M110.000299).
[42] A. Olteanu, C.N. Patel, M.M. Dedmon, S. Kennedy, M.W. Linhoff, C.M. Minder, P.R. Potts, M. Deshmukh, G.J. Pielak, Stability and apoptotic activity of recombinant human cytochrome c, Biochem. Biophys. Res. Commun. 312 (2003) 733–740.
[43] S.M. Kelly, T.J. Jess, N.C. Price, How to study proteins by circular dichroism, Biochim. Biophys. Acta – Proteins Proteomics 1751 (2005) 119–139.
[44] N. Sreerama, R.M. Woody, Estimation of protein secondary structure from CD spectra: comparison of CONTIN, SELCON and CDSSTR methods with an expanded reference set, Anal. Biochem. 282 (2000) 252–260.
[45] N.J. Greenfield, Using circular dichroism spectra to estimate protein secondary structure, Nat. Protoc. 1 (2007) 2876–2890.
[46] G. Blauer, N. Sreerama, R.W. Woody, Optical activity of hemeproteins in the Soret region. Circular dichroism of the heme undecapeptide of cytochrome c in aqueous solution, Biochemistry 32 (1993) 6674–6679.
[47] B. Ranjbar, P. Gill, Circular dichroism techniques: biomolecular and nanostructural analyses — a review, Chem. Biol. Drug Des. 74 (2009) 101–120.
[48] R.E. Dickerson, R. Timkovich, in: P.D. Boyer (Ed.), The Enzymes, third ed., Vol. 11, Academic Press, New York 1975, pp. 397–547.
[49] P.L. Dutton, D.F. Wilson, Redox potentiometry in mitochondrial and photosynthetic bioenergetics, Biochim. Biophys. Acta, Bioenerg. 346 (1974) 165–212.
[50] V. Rodríguez-Roldán, J.M. García-Heredia, J.A. Navarro, M.A. De la Rosa, M. Hervás, Effect of nitration on the physicochemical and kinetic features of wild-type and monotyrosine mutants of human respiratory cytochrome c. Biochemistry 47 (2008) 12371–12379.
[51] D.H. Case, T.A. Darden, T.E. Cheatham, C.L. Simmerling, J. Wang, R.E. Duke, R. Luo, R.C. Walker, W. Zhang, K.M. Merz., B. Roberts, S. Hayik, A. Roitberg, G. Seabra, J. Swails, A.W. Goetz, I. Kolossváry, K.F. Wong, F. Paesani, J. Vanicek, R.M. Wolf, J. Liu, X. Wu, S.R. Brozell, T. Steinbrecher, H. Gohlke, Q. Cai, X. Ye, J. Wang, M.J. Hsieh, G. Cui, D.R. Roe, D.H. Mathews, M.G. Seetin, R. Salomon-Ferrer, C. Sagui, V. Babin, T. Luchko, S. Gusarov, A. Kovalenko, P.A. Kollman, AMBER 12, University of California, San Francisco (USA), 2012.
[52] W.D. Cornell, P. Cieplak, C.I. Bayly, I.R. Gould, K.M. Merz, D.M. Ferguson, D.C. Spellmeyer, T. Fox, J.W. Caldwell, P.A. Kollman, A second generation force field for the simulation of proteins, nucleic acids, and organic molecules, J. Am. Chem. Soc. 117 (1995) 5179–5197;
J. Am. Chem. Soc. 118 (1996) 2309.
[53] F. Autenrieth, E. Tajkhorshid, J. Baudry, Z. Luthey-Schulten, Classical force field parameters for the heme prosthetic group of cytochrome c, J. Comput. Chem. 25 (2004) 1613–1622.
[54] B.S. Rajagopal, A.N. Edzuma, M.A. Hough, K.L.I.M. Blundell, V.E. Kagan, A.A. Kapralov, L.A. Fraser, J.N. Butt, G.G. Silkstone, G.G. Wilson, D.A. Svistunenko, J.A. Worrall, The hydrogen-peroxide-induced radical behaviour in human cytochrome c–phospholipid complexes: implications for the enhanced pro-apoptotic activity of the G41S mutant, Biochem. J. 456 (2013) 441–452.
[55] L. Banci, P. Carloni, A. DÍaz, G. Gori Savellini, Molecular dynamics calculations on peroxidases: the effect of calcium ions on protein structure, J. Biol. Inorg. Chem. 1 (1996) 264–272.
[56] L. Banci, I. Bertini, H.B. Gray, C. Luchinat, T. Reddig, A. Rosato, P. Turano, Solution structure of oxidized horse heart cytochrome c, Biochemistry 36 (1997) 9867–9877.
[57] R. Santucci, F. Ascoli, The Soret circular dichroism spectrum as a probe for the heme Fe(III)-Met(80) axial bond in horse cytochrome c. J. Inorg. Biochem. 68 (1997) 211–214.
[58] R. Schweitzer-Stenner, Internal electric field in cytochrome c explored by visible electronic circular dichroism spectroscopy, J. Phys. Chem. B 112 (2008) 10358–10366.
[59] M.D. Liptak, R.D. Fagerlund, E.C. Ledgerwood, S.M. Wilbanks, K.L. Bren, The proapoptotic G41S mutation to human cytochrome c alters the heme electronic structure and increases the electron self-exchange rate, J. Am. Chem. Soc. 133 (2011) 1153–1155.
[60] R. Schweitzer-Stenner, Internal electric field in cytochrome c explored by visible electronic circular dichroism spectroscopy, J. Phys. Chem. B 112 (2008) 10358–10366.
[61] F. Boffi, A. Bonincontro, S. Cinelli, A. Congiu Castellano, A. A. De Francesco, S. Della Longa, M. Girasole, G. Onori, pH-Dependent local structure of ferricytochrome c studied by X-ray absorption spectroscopy, Biophys. J. 80 (2001) 149–1473.
[62] T. Ying, F. Zhong, J. Xie, Y. Feng, Z.H. Wang, Z.X. Huang, X. Tan, Evolutionary alkaline transition in human cytochrome c. J. Bioenerg. Biomembr. 41 (2009) 251–257.
[63] M.T. Wilson, C. Greenwood, in: R.A. Scott, A.G. Mauk (Eds.), Cytochrome c: A Multidisciplinary Approach, University Science Books, Sausilito 1996, pp. 611–634.
[64] M. Assfalg, I. Bertini, A. Dolfi, P. Turano, A.G. Mauk, F.I. Rosell, H.B. Gray, Structural model for an alkaline form of ferricytochrome c, J. Am. Chem. Soc. 125 (2003) 2913–2922.
[65] L.C. Godoy, C. Muñoz-Pinedo, L. Castro, S. Cardaci, C.M. Schonhoff, M. King, V. Tórtora, M. Marín, Q. Miao, J.F. Jiang, A. Kapralov, R. Jemmerson, G.G. Silkstone, J.N. Patel, J.E. Evans, M.T. Wilson, D.R. Green, V.E. Kagan, R. Radi, J.B. Mannick, Disruption of the M80-Fe ligation stimulates the translocation of cytochrome c to the cytoplasm and nucleus in nonapoptotic cells, Proc. Natl. Acad. Sci. U. S. A. 106 (2009) 2653–2658.
[66] A. Schejter, P. George, The 695-mμ band of ferricytochrome c and its relationship to protein conformation, Biochemistry 3 (1964) 1045–1049.
[67] T.L. Poulos, The role of the proximal ligand in heme enzymes, J. Biol. Inorg. Chem. 1 (1996) 356–359.
[68] A. Lawrence, C.M. Jones, P. Wardman, M.J. Burkitt, Evidence for the role of a peroxidase compound I-type intermediate in the oxidation of glutathione, NADH, ascorbate, and dichlorofluorescin by cytochrome c/H_2O_2 implications for oxidative stress during apoptosis, J. Biol. Chem. 278 (2003) 29410–29419.
[69] L.J. McClelland, T.C. Mou, M.E. Jeakins-Cooley, S.R. Sprang, B.E. Bowler, Structure of a mitochondrial cytochrome c conformer competent for peroxidase activity, Proc. Natl. Acad. Sci. U. S. A. 111 (2014) 6648–6653.
[70] L.A. Pandiscia, R. Schweitzer-Stenner, Coexistence of native-like and non-native cytochrome c on anionic liposomes with different cardiolipin content, J. Phys. Chem. B 119 (2015) 1334–1349.
[71] I. Bertini, S. Chevance, R. Del Conte, D. Lalli, P. Turano, The anti-apoptotic Bcl-xL protein, a new piece in the puzzle of cytochrome c interactome, PLoS One 6 (2011), e18329.
[72] I.M. Morison, E.M. Cramer Bordé, E.J. Cheesman, P.L. Cheong, A.J. Holyoake, S. Fichelson, R.J. Weeks, A. Lo, S.M. Davies, S.M. Wilbanks, R.D. Fagerlund, M.W. Ludgate, F.M. da Silva Tatley, M.S. Coker, N.A. Bockett, G. Hughes, D.A. Pippig, M.P. Smith, C. Capron, E.C. Ledgerwood, A mutation of human cytochrome c enhances the intrinsic apoptotic pathway but causes only thrombocytopenia, Nat. Genet. 40 (2008) 387–389.
[73] E. Solary, F. Giordanetto, G. Kroemer, Re-examining the role of cytochrome c in cell death, Nat. Genet. 40 (2008) 379–380.
[74] A.I. Karsisiotis, O.M. Deacon, B.S. Rajagopal, C. Macdonald, T.M. Blumenschein, G.R. Moore, J.A. Worrall, Backbone resonance assignments of ferric human cytochrome c and the pro-apoptotic G41S mutant in the ferric and ferrous states, Biomol. NMR Assign. 9 (2015) 415–419.
[75] B.S. Rajagopal, A.N. Edzuma, M.A. Hough, K.L. Blundell, V.E. Kagan, A.A. Kapralov, L.A. Fraser, J.N. Butt, G.G. Silkstone, M.T. Wilson, D.A. Svistunenko, J.A. Worrall, The hydrogen-peroxide-induced radical behaviour in human cytochrome c-phospholipid complexes: implications for the enhanced pro-apoptotic activity of the G41S mutant, Biochem. J. 456 (2013) 441–452.